arXiv:1603.02137v1 [quant-ph] 7 Mar 2016

Spectrum analysis with quantum dynamical systems

Shilin Ng,[1] Shan Zheng Ang,[2] Trevor A. Wheatley,[3,4] Hidehiro Yonezawa,[3,4]
Akira Furusawa,[5] Elanor H. Huntington,[4,6] and Mankei Tsang[2,1,*]

[1] *Department of Physics, National University of Singapore, 2 Science Drive 3, Singapore 117551*
[2] *Department of Electrical and Computer Engineering, National University of Singapore, 4 Engineering Drive 3, Singapore 117583*
[3] *School of Engineering and Information Technology, University of New South Wales Canberra, ACT 2600, Australia*
[4] *Centre for Quantum Computation and Communication Technology, Australian Research Council*
[5] *Department of Applied Physics, School of Engineering, The University of Tokyo, 7-3-1 Hongo, Bunkyo-ku, Tokyo 113-8656, Japan*
[6] *Research School of Engineering, College of Engineering and Computer Science, Australian National University, North Road, Acton, Canberra ACT 2600, Australia*

(Dated: March 8, 2016)

Measuring the power spectral density of a stochastic process, such as a stochastic force or magnetic field, is a fundamental task in many sensing applications. Quantum noise is becoming a major limiting factor to such a task in future technology, especially in optomechanics for temperature, stochastic gravitational wave, and decoherence measurements. Motivated by this concern, here we prove a measurement-independent quantum limit to the accuracy of estimating the spectrum parameters of a classical stochastic process coupled to a quantum dynamical system. We demonstrate our results by analyzing the data from a continuous optical phase estimation experiment and showing that the experimental performance with homodyne detection is close to the quantum limit. We further propose a spectral photon counting method that can attain quantum-optimal performance for weak modulation and a coherent-state input, with an error scaling superior to that of homodyne detection at low signal-to-noise ratios.

I. INTRODUCTION

Recent technological advances, especially in optomechanics [1], suggest that quantum noise will soon be the major limiting factor in many metrological applications [2]. Many tasks in optomechanics force sensing, including thermometry, estimation of stochastic gravitational-wave background [3], and testing spontaneous wavefunction collapse [4, 5], involve the spectrum analysis of a stochastic force, and the effect of quantum noise on such tasks has been of recent interest [4, 5]. To study the quantitative effect of experimental design on estimation accuracy, it is important to use a rigorous statistical inference framework to investigate the parameter estimation error. While there exist many theoretical studies of quantum parameter estimation for thermometry (see, for example, Refs. [6–10]), their application to more complex dynamical systems with broadband measurements such as optomechanics remains unclear.

In this work, we propose a theoretical framework of spectrum-parameter estimation with quantum dynamical systems, proving fundamental limits and investigating measurement and data analysis techniques that approach the limits. An outstanding feature of our work is the simple analytic results in terms of basic power spectral densities (PSDs) in the problem, such that they can be readily applied to optics and optomechanics experiments. To illustrate our theory, we analyze a recent experiment of continuous optical phase estimation and demonstrate that the experimental performance using homodyne detection is close to our quantum limit. We further propose a spectral photon counting method that can beat homodyne detection and attain quantum-optimal performance for weak modulation and a coherent-state input. The advantage is especially significant when the signal-to-noise ratio (SNR) is low, thus demonstrating the importance of quantum-optimal measurements and coherent optical information processing in the low-SNR regime for gravitational-wave astronomy [11] and optical sensing in general.

II. QUANTUM METROLOGY

A. Parameter estimation

Consider a quantum dynamical system with Hamiltonian $\hat{H}[X,t]$ as a functional of a c-number hidden stochastic process $X(t)$, such as a classical force. Assume that the prior probability measure of $X(t)$ depends on a vector of unknown parameters θ. Let Y be the quantum measurement outcome and $\check{\theta}(Y)$ be an estimator of θ using Y. The central error figure of interest is the mean-square estimation error matrix, defined as

$$\Sigma_{\mu\nu}(\theta) \equiv \mathbb{E}_Y \left\{ \left[\check{\theta}_\mu(Y) - \theta_\mu\right] \left[\check{\theta}_\nu(Y) - \theta_\nu\right] \right\}, \qquad (2.1)$$

with $\mathbb{E}_Y$ denoting the expectation over the random variable Y. Our goal here is to compute analytic results

* mankei@nus.edu.sg

concerning Σ and discover quantum measurement techniques that can accurately estimate θ.

For any unbiased estimator ($\mathbb{E}_Y(\hat{\theta}) = \theta$), the multiparameter Cramér-Rao bound states that

$$\Sigma \geq j^{-1}(P_Y), \tag{2.2}$$

where $j(P_Y)$ is the classical Fisher information matrix with respect to the observation probability measure P_Y [12]. The matrix inequality means that $\Sigma - j^{-1}$ is positive-semidefinite, that is, $u_\mu(\Sigma - j^{-1})_{\mu\nu}u_\nu \geq 0$ for any real vector u (Einstein summation is assumed throughout this paper). For a quantum system, let $\hat{\rho}(\theta)$ be a θ-dependent density operator and $\hat{E}(y)$ be the positive operator-valued measure (POVM) that models the measurement, such that

$$P_Y(y|\theta) = \mathrm{tr}\left[\hat{E}(y)\hat{\rho}(\theta)\right], \tag{2.3}$$

with tr being the operator trace. For dynamical systems, $\hat{\rho}(\theta)$ can be obtained using the principles of purification and deferred measurements [13–16]. For the purpose of spectrum-parameter estimation, we model $\hat{\rho}$ as

$$\hat{\rho}(\theta) = \mathbb{E}_{X|\theta}\left\{\hat{U}[X,T]|\psi\rangle\langle\psi|\hat{U}^\dagger[X,T]\right\}, \tag{2.4}$$

where

$$\hat{U}[X,T] = \mathcal{T}\exp\left\{-\frac{i}{\hbar}\int_0^T dt\hat{H}[X,t]\right\} \tag{2.5}$$

is the unitary time-ordered exponential of $\hat{H}$ with total evolution time T, $|\psi\rangle$ is the initial quantum state, and the expectation is with respect to the hidden process $X(t)$, the prior probability measure of which depends on θ. θ is called hyperparameters in this context [17]. For any POVM, a quantum Cramér-Rao bound states that

$$j(P_Y) \leq J(\hat{\rho}), \tag{2.6}$$

where $J(\hat{\rho})$ is the quantum Fisher information matrix with respect to the symmetric logarithmic derivatives of $\hat{\rho}$ [18–20].

B. Extended convexity

While quantum parameter estimation bounds for dynamical systems have been studied previously in the context of low-dimensional systems such as qubits (see, for example, Refs. [21–23]), J is much more difficult to evaluate analytically for multimode high-dimensional dynamical systems under continuous measurements. To proceed, we exploit a recently discovered property of J known as the extended convexity [24], which states that

$$J(\hat{\rho}) \leq \mathcal{J}\{\hat{\sigma}, P_Z\} \equiv \mathbb{E}_{Z|\theta}\left[J(\hat{\sigma})\right] + j(P_Z), \tag{2.7}$$

where $\{\hat{\sigma}, P_Z\}$ is any ensemble of $\hat{\rho}$ with elements $\hat{\sigma}$ and mixing probability measure P_Z such that $\hat{\rho}(\theta) = \mathbb{E}_{Z|\theta}[\hat{\sigma}(Z|\theta)]$.

The proof of extended convexity $J \leq \mathcal{J}$ for one parameter in Ref. [24] relies on the assumption that there exists an optimal POVM attaining $j = J$. Such an assumption is questionable however [25], and here we use instead the strong concavity of Uhlmann fidelity [13] to prove Eq. (2.7) for multiple parameters. Let $\{\hat{\sigma}, P_Z\}$ be an ensemble for $\hat{\rho}(\theta)$ such that

$$\hat{\rho}(\theta) = \int dz P_Z(z|\theta)\hat{\sigma}(z|\theta). \tag{2.8}$$

Define the Uhlmann fidelity as

$$F[\hat{\rho}, \hat{\rho}'] \equiv \mathrm{tr}\sqrt{\sqrt{\hat{\rho}}\hat{\rho}'\sqrt{\hat{\rho}}}. \tag{2.9}$$

The strong concavity states that [13]

$$F\left[\hat{\rho}(\theta), \hat{\rho}(\theta')\right] \geq \int dz\sqrt{P_Z(z|\theta)P_Z(z|\theta')} \times F[\hat{\sigma}(z|\theta), \hat{\sigma}(z|\theta')]. \tag{2.10}$$

To relate F to J, we use the fact [20]

$$F[\hat{\rho}(\theta), \hat{\rho}(\theta + \epsilon u)] = 1 - \frac{\epsilon^2}{8}u_\mu J_{\mu\nu}(\hat{\rho})u_\nu + o(\epsilon^2), \tag{2.11}$$

where ϵ is a scalar, u is any real vector with the same dimension as θ, and $o(\epsilon^2)$ denotes terms asymptotically smaller than ϵ^2. It is also known that [26]

$$\int dz\sqrt{P_Z(z|\theta)P_Z(z|\theta + \epsilon u)} = 1 - \frac{\epsilon^2}{8}u_\mu j_{\mu\nu}(P_Z)u_\nu + o(\epsilon^2). \tag{2.12}$$

Expanding $F[\hat{\rho}(\theta), \hat{\rho}(\theta')]$ and $F[\hat{\sigma}(z|\theta), \hat{\sigma}(z|\theta')]$ in Eq. (2.10) using Eq. (2.11), applying Eq. (2.12) to the right-hand side of Eq. (2.10), and comparing the ϵ^2 terms on both sides, we obtain

$$u_\mu J_{\mu\nu}(\hat{\rho})u_\nu \leq u_\mu\left\{\mathbb{E}_{Z|\theta}\left[J_{\mu\nu}(\hat{\sigma})\right] + j_{\mu\nu}(P_Z)\right\}u_\nu. \tag{2.13}$$

Since this holds for any u, we obtain the matrix inequality in Eq. (2.7). The classical simulation technique proposed in Ref. [27] can be regarded as a special case of extended convexity when $J(\hat{\sigma}) = 0$.

C. Dynamical systems

To compute simple analytic results for dynamical systems, we make further assumptions. Assume that $X(t)$ is zero-mean, Gaussian, and stationary, with a PSD given by

$$S_X(\omega|\theta) \equiv \int_{-\infty}^{\infty} d\tau\mathbb{E}_{X|\theta}[X(t)X(t+\tau)]\exp(i\omega\tau). \tag{2.14}$$

For the quantum system, we assume that the Hamiltonian is of the form

$$\hat{H} = \hat{H}_0 - \hat{Q}X(t), \tag{2.15}$$

where $\hat{Q}$ is the quantum generator and $\hat{H}_0$ is the rest of the Hamiltonian. For example, $X(t)$ can be the classical force on a mechanical oscillator and $\hat{Q}$ can be the quantum position operator, as depicted in Fig. 1(a).

A modified purification technique can transform the problem in the interaction picture and produce an alternative and possibly tighter bound in terms of the optical statistics alone [16]. For an optomechanical system, the Hamiltonian is of the form [1]

$$\hat{H}_{\rm OM} = \hat{H}_{\rm M} + \hat{H}_{\rm O} + \hat{h}, \tag{2.16}$$

where $\hat{H}_{\rm M}$ is the mechanical Hamiltonian, $\hat{H}_{\rm O}$ is the optical Hamiltonian, and $\hat{h}$ is the optomechanical interaction Hamiltonian. For example, if the mechanical oscillator with position operator $\hat{q}$ interacts with one cavity optical mode with photon-number operator $\hat{n}$, $\hat{h} = -\hbar g_0 \hat{n}\hat{q}$, where g_0 is a coupling constant. A classical force $f(t)$ on the mechanical oscillator leads to a term $-\hat{q}f(t)$ in $\hat{H}_{\rm M}$, and if we assume $\hat{U}$ to be the time-ordered exponential of $\hat{H}_{\rm OM}$, $f(t)$ can be regarded as the hidden process and $\hat{q}$ the generator.

In practice, measurements are made on the optics and not the mechanics directly, so one is free to modify the purification [28] by applying any mechanical unitary to the optomechanical one [16]. To be specific, let $\hat{U}_{\rm OM}$ be the time-ordered exponential of $\hat{H}_{\rm OM}$ and $\hat{U}_{\rm M}$ be the time-ordered exponential of $\hat{H}_{\rm M}$. Since the POVM is not applied to the mechanics, $\hat{U}|\psi\rangle\langle\psi|\hat{U}^\dagger$ with $\hat{U} = \hat{U}_{\rm M}^\dagger \hat{U}_{\rm OM}$ is also a valid purification for a given force [16]. $\hat{U}$ becomes the time-ordered exponential of the interaction-picture Hamiltonian

$$\hat{H}(t) = \hat{H}_{\rm O} + \hat{h}_{\rm M}(t), \quad \hat{h}_{\rm M}(t) \equiv \hat{U}_{\rm M}^\dagger(t)\hat{h}\hat{U}_{\rm M}(t). \tag{2.17}$$

For cavity optomechanics, $\hat{h}_{\rm M}(t) = -\hbar g_0 \hat{n}\hat{q}_{\rm M}(t)$, where $\hat{q}_{\rm M}(t)$ is the interaction-picture mechanical position. For a linear mechanical system, $\hat{q}_{\rm M}(t) = \hat{q}_0(t) + X(t)$, where $\hat{q}_0(t)$ is the operator-valued homogeneous component as a function of the initial position and momentum operators and $X(t)$ is the c-number inhomogeneous component of the displacement due to the classical force. We can hence take $X(t)$ to be the hidden process and $\hat{Q} = \hbar g_0 \hat{n}$ to be the generator, obtaining uncertainty relations between the displacement errors and the photon-number fluctuations, as depicted in Fig. 1(b).

In general, this interaction-picture purification method can be applied to any linear system with Hamiltonian of the form $\hat{H}_0 - \hat{Q}X(t)$, where $\hat{Q}$ is a canonical coordinate operator and $\hat{H}_0$ is quadratic with respect to canonical coordinates, as the effect of $X(t)$ remains a displacement operation in any interaction picture.

Figure 1(c) and (d) depict two other examples of Eq. (2.15) in the context of optical phase modulation, in which case $X(t)$ is the phase modulation on the optical beam and $\hat{Q}$ is proportional to the photon-flux operator. Other examples include the magnetometer, where $X(t)$ is an external magnetic field and $\hat{Q}$ is a spin operator [29], and the voltmeter, where $X(t)$ is an applied voltage and $\hat{Q}$ is a charge operator.

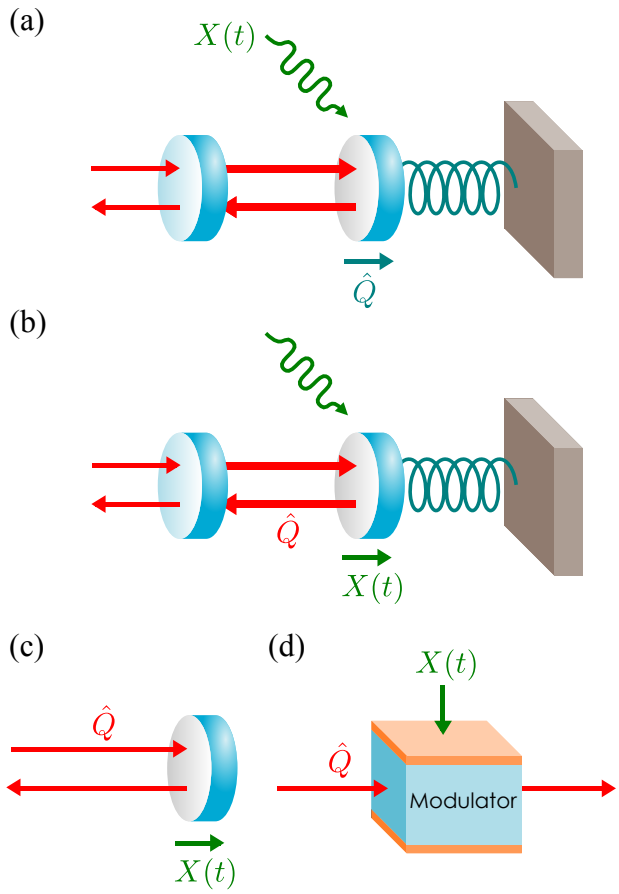

FIG. 1. (Color online). Some examples of the hidden stochastic process $X(t)$ and generator $\hat{Q}$. (a) $X(t)$ is the classical force and $\hat{Q}$ is the mechanical position, (b) $X(t)$ is the c-number forced displacement and $\hat{Q}$ is proportional to the photon-number operator, (c) and (d) $X(t)$ is the phase modulation and $\hat{Q}$ is proportional to the photon-flux operator.

D. Variational bound

As the extended convexity holds for any ensemble of $\hat{\rho}$, tighter bounds can be obtained by choosing the ensemble judiciously [24]. Instead of the original ensemble given by Eq. (2.4), we define a new stochastic process $Z(t)$ by

$$X(t) = \int_{-\infty}^{\infty} d\tau g(t-\tau|\theta)Z(\tau), \tag{2.18}$$

where g is an impulse-response function to be chosen later. $\hat{\rho}$ can now be expressed as

$$\hat{\rho}(\theta) = \mathbb{E}_{Z|\theta}\left\{\hat{U}[g*Z,T]|\psi\rangle\langle\psi|\hat{U}^\dagger[g*Z,T]\right\}, \quad (2.19)$$

where $*$ denotes convolution. With

$$\hat{\sigma} = \hat{U}[g*Z,T]|\psi\rangle\langle\psi|\hat{U}^\dagger[g*Z,T], \quad (2.20)$$

this results in a family of ensembles $\{\hat{\sigma}, P_Z\}$ parameterized by g for a given $\hat{\rho}$.

Assuming the Hamiltonian in Eq. (2.15), it can be shown that [14, 30]

$$\begin{aligned} J_{\mu\nu}(\hat{\sigma}) = \frac{4}{\hbar^2}\int_0^T dt \int_0^T dt' K_Q(t,t') \\ \times \int_{-\infty}^{\infty} d\tau \partial_\mu g(t-\tau|\theta) Z(\tau) \\ \times \int_{-\infty}^{\infty} d\tau' \partial_\nu g(t'-\tau'|\theta) Z(\tau'), \end{aligned} \quad (2.21)$$

where $\partial_\mu \equiv \partial/\partial\theta_\mu$ and $K_Q(t,t')$ is the quantum covariance of the generator in the Heisenberg picture, defined as

$$K_Q(t,t') \equiv \mathrm{Re}\left[\langle\psi|\Delta\hat{Q}(t)\Delta\hat{Q}(t')|\psi\rangle\right], \quad (2.22)$$

$$\Delta\hat{Q}(t) \equiv \hat{Q}(t) - \langle\psi|\hat{Q}(t)|\psi\rangle, \quad (2.23)$$

$$\hat{Q}(t) \equiv \hat{U}^\dagger(X,t)\hat{Q}\hat{U}(X,t). \quad (2.24)$$

We now assume that $K_Q(t,t')$ is independent of $X(t)$; such an assumption is commonly satisfied in linear optomechanics and optical-phase-modulation systems. The expected $J(\hat{\sigma})$ becomes

$$\begin{aligned} \mathbb{E}_{Z|\theta}\left[J_{\mu\nu}(\hat{\sigma})\right] = \frac{4}{\hbar^2}\int_0^T dt \int_0^T dt' K_Q(t,t') \\ \times \int_{-\infty}^{\infty} d\tau \int_{-\infty}^{\infty} d\tau' K_Z(\tau,\tau'|\theta) \\ \times \left[\partial_\mu g(t-\tau|\theta)\right]\left[\partial_\nu g(t'-\tau'|\theta)\right], \end{aligned} \quad (2.25)$$

where

$$K_Z(\tau,\tau'|\theta) \equiv \mathbb{E}_{Z|\theta}\left[Z(\tau)Z(\tau')\right] \quad (2.26)$$

is the prior covariance of $Z(t)$. Assume further that the quantum statistics of $\Delta\hat{Q}(t)$ are stationary, with a PSD given by

$$S_Q(\omega) \equiv \int_{-\infty}^{\infty} d\tau K_Q(t,t+\tau)\exp(i\omega\tau). \quad (2.27)$$

The assumption of stationary processes and a long observation time T (relative to all other time scales in the problem) is known as the SPLOT assumption. Defining a transfer function as

$$G(\omega|\theta) \equiv \int_{-\infty}^{\infty} dt g(t|\theta)\exp(i\omega t), \quad (2.28)$$

restricting G to be nonzero for all frequencies of interest, noting that the PSD of $Z(t)$ is $S_X/|G|^2$, and making the SPLOT assumption, Eq. (2.25) can be rewritten as

$$\mathbb{E}_{Z|\theta}\left[J_{\mu\nu}(\hat{\sigma})\right] = T\int_{-\infty}^{\infty}\frac{d\omega}{2\pi}\frac{4S_Q S_X}{\hbar^2}\left(\partial_\mu \ln G\right)\left(\partial_\nu \ln G^*\right). \quad (2.29)$$

The Fisher information $j(P_Z)$ can be obtained by applying Eq. (2.12) to the Bhattacharyya distance between two stationary Gaussian processes [31]. The result is

$$j_{\mu\nu}(P_Z) = T\int_{-\infty}^{\infty}\frac{d\omega}{2\pi}\frac{1}{2}\left(\partial_\mu \ln\frac{S_X}{|G|^2}\right)\left(\partial_\nu \ln\frac{S_X}{|G|^2}\right). \quad (2.30)$$

Combining Eqs. (2.29) and (2.30) according to Eq. (2.7), we obtain

$$\begin{aligned} u_\mu \mathcal{J}_{\mu\nu} u_\nu = T\int_{-\infty}^{\infty}\frac{d\omega}{2\pi}\left[\frac{4S_Q S_X}{\hbar^2}|\lambda|^2 + \frac{1}{2}\left(\Lambda - \lambda - \lambda^*\right)^2\right], \\ \lambda \equiv u_\mu\partial_\mu \ln G, \quad \Lambda \equiv u_\mu \partial_\mu \ln S_X. \end{aligned} \quad (2.31)$$

Since Eq. (2.31) is quadratic with respect to λ, the λ and thus G that minimizes Eq. (2.31) for each u can be found analytically. Straightforward algebra then leads to a variational upper bound on the quantum Fisher information given by

$$J \le \tilde{\mathcal{J}}, \quad \tilde{\mathcal{J}}_{\mu\nu} \equiv T\int_{-\infty}^{\infty}\frac{d\omega}{2\pi}\frac{(\partial_\mu \ln S_X)(\partial_\nu \ln S_X)}{2+\hbar^2/(S_Q S_X)}. \quad (2.32)$$

This is the first main result of this paper. Note that the quantum state $|\psi\rangle$ need not be Gaussian for the result to hold.

For mechanical force measurements, the straightforward choice of the Hamiltonian leads to S_X being the force PSD and S_Q being the mechanical position PSD. For linear cavity optomechanics, the interaction-picture purification technique explained in Sec. II C leads to an alternative Hamiltonian such that S_X is the PSD of the forced displacement and S_Q is proportional to the cavity photon-number PSD. For continuous optical phase modulation [32–35], S_X is the phase PSD and $S_Q/\hbar^2$ is the photon-flux PSD. In all cases, the frequency-domain integral given by Eq. (2.32), together with the matrix inequalities

$$\Sigma \ge j^{-1} \ge J^{-1} \ge \tilde{\mathcal{J}}^{-1} \quad (2.33)$$

that follow from Eqs. (2.2), (2.6), and (2.32), represent a novel form of uncertainty relations and indicate a nontrivial interplay between the classical noise characterized by S_X and a frequency-domain SNR given by $S_Q S_X/\hbar^2$ in bounding the estimation error and the Fisher information quantities. Note also that $\tilde{\mathcal{J}}$ is proportional to the total time T, as are all the Fisher information quantities we derive here. This means that a longer observation time can improve the parameter estimation even if the SNR is low, as is well known in statistics [36] but missed by some of the previous quantum studies [4, 5].

III. CONTINUOUS OPTICAL PHASE MODULATION

A. Error bounds

To illustrate our theory, consider the optics experiment depicted in Fig. 1(c) or (d). An external stochastic source $X(t)$, such as a moving mirror or an electro-optic modulator, modulates the phase of a continuous optical beam, which is then measured to obtain information about the source. The Hamiltonian is

$$\hat{H} = \hbar \hat{I}(t) X(t), \tag{3.1}$$

where $\hat{I}(t)$ is the photon-flux operator, $S_X(\omega|\theta)$ is the source PSD, and $S_I(\omega) = S_Q(\omega)/\hbar^2$ is the photon-flux PSD. This model also applies to quantum optomechanics if the dynamics can be linearized around a strong optical mean field and a suitable interaction picture is used, as discussed in Sec. II C. The quantum limit given by Eq. (2.32) becomes

$$\tilde{\mathcal{J}}_{\mu\nu} = T \int_{-\infty}^{\infty} \frac{d\omega}{2\pi} \frac{(\partial_\mu \ln S_X)(\partial_\nu \ln S_X)}{2 + 1/(S_I S_X)}. \tag{3.2}$$

Equation (3.2) together with Eq. (2.33) represent an uncertainty relation between the phase spectrum-parameter estimation error and the photon-flux PSD.

We can compare our bound with the Fisher information for homodyne detection, a standard experimental phase measurement method [32–35], as illustrated in Fig. 2(a). If the mean field is strong, and the modulation is weak or tight phase locking is achieved, the output process can be linearized as

$$Y(t) \approx X(t) + \eta(t), \tag{3.3}$$

where $\eta(t)$ is the phase-quadrature noise. The information $j(P_Y^{(\mathrm{hom})})$ can be computed analytically if η is Gaussian and stationary with power spectral density $S_\eta(\omega)$ such that Y is also Gaussian and stationary [31]; the result with the SPLOT assumption is

$$j_{\mu\nu}\left(P_Y^{(\mathrm{hom})}\right) = T \int_{-\infty}^{\infty} \frac{d\omega}{2\pi} \frac{(\partial_\mu \ln S_X)(\partial_\nu \ln S_X)}{2(1 + S_\eta/S_X)^2}. \tag{3.4}$$

The classical Cramér-Rao bound $\Sigma \geq j^{-1}(P_Y^{(\mathrm{hom})})$ is asymptotically attainable for long T using maximum-likelihood estimation [36].

With the quadrature uncertainty relation

$$S_\eta(\omega) S_I(\omega) \geq \frac{1}{4} \tag{3.5}$$

for the optical beam [37], the optimal homodyne information is

$$j\left(P_Y^{(\mathrm{hom})}\right) \leq \tilde{j},$$
$$\tilde{j}_{\mu\nu} \equiv T \int_{-\infty}^{\infty} \frac{d\omega}{2\pi} \frac{(\partial_\mu \ln S_X)(\partial_\nu \ln S_X)}{2 + 1/(S_I S_X) + 1/(8 S_I^2 S_X^2)}. \tag{3.6}$$

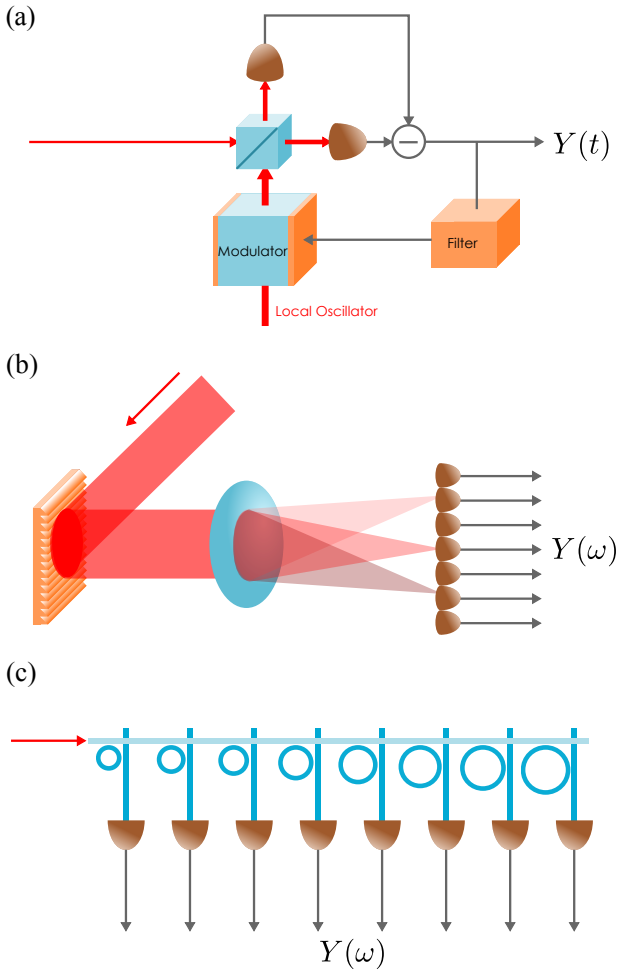

FIG. 2. (Color online). (a) Adaptive homodyne detection. (b) Spectral photon counting with a diffraction grating and a lens. (c) Spectral photon counting with an optical-resonator array.

We can compare this homodyne limit with the quantum limit in Eq. (3.2); the expressions are similar, apart from a extra factor of $1/(8S_I^2 S_X^2)$ that makes the homodyne limit strictly worse than our quantum limit, especially if $S_I S_X$ is small.

B. Spectral photon counting

Although Eq. (2.33) sets rigorous lower bounds on the estimation error Σ, there is no guarantee that the the error for any measurement can attain the final bound $\tilde{J}^{-1}$. Inspired by our previous work on astronomical quantum optics [10, 38], here we analyze an alternative measurement that we call spectral photon counting. Physically, it is simply a conventional optical spectrometer with photon counting for each spectral mode [39, 40]. The first step of spectral photon counting is the coherent optical Fourier transform via a dispersive optical element, such as a diffraction grating or a prism and a Fourier-

transform lens [39] as depicted in Fig. 2(b), or an array of optical ring resonators with different resonant frequencies coupled to a cross grid of waveguides [41] as depicted in Fig. 2(c). The second step is a measurement of the photon numbers in the spectral modes, and the final step is a maximum-likelihood estimation of θ from the spectral photon counting results. For the phase spectrum-parameter estimation problem with weak modulation and a coherent-state input, this method turns out to have an information $j(P_Y^{(\mathrm{spc})})$ coinciding with $\tilde{\mathcal{J}}$ for all parameters.

Let the positive-frequency electric field at the input of the phase modulator be

$$\hat{E}^{(+)}(t) = \hat{A}(t)\exp(-i\Omega t), \tag{3.7}$$

where $\hat{A}(t)$ is an annihilation operator for the slowly varying envelope with commutation relation

$$[\hat{A}(t), \hat{A}^\dagger(t')] = \delta(t-t'), \tag{3.8}$$

and Ω is the optical carrier frequency. With a strong mean field

$$\alpha \equiv \langle\psi|\hat{A}(t)|\psi\rangle \tag{3.9}$$

and weak phase modulation, the output field can be linearized as

$$\hat{B}(t) \approx \hat{A}(t) + i\alpha X(t). \tag{3.10}$$

To model the optical Fourier transform, we follow Shapiro [39] to express each frequency mode in terms of the mode annihilation operator as

$$\hat{b}_m = \frac{1}{\sqrt{T}}\int_0^T dt\hat{B}(t)\exp(i\omega_m t), \tag{3.11}$$

with sideband frequencies

$$\omega_m = \frac{2\pi m}{T}, \quad m \in \{\dots,-2,-1,0,1,2,\dots\}, \tag{3.12}$$

and

$$[\hat{b}_m, \hat{b}_n^\dagger] = \delta_{mn}. \tag{3.13}$$

Assuming α to be time-constant,

$$\hat{b}_m \approx \hat{a}_m + i\alpha x_m, \tag{3.14}$$

where $\hat{a}_m$ is the Fourier transform of $\hat{A}(t)$ and x_m is that of $X(t)$ in the same way as $\hat{b}_m$.

The strong mean field is contained in the $m=0$ mode only, and if the spectrum of x_m is wide, negligible information is lost if we neglect the $m=0$ mode. The other modes are coherent states for a given displacement $i\alpha x_m$ if the input beam is a coherent state [39]. For a given x_m, the photon-counting distribution for $\hat{n}_m \equiv \hat{b}_m^\dagger\hat{b}_m$ in each mode is therefore Poissonian with mean $|\alpha|^2|x_m|^2$ and independent from one another.

Since $X(t)$ is a hidden stochastic process, we must average the Poissonian distribution over the prior of $X(t)$ to obtain the final likelihood function. For a Gaussian $X(t)$ with the SPLOT assumption, $\{x_m; m>0\}$ are independent complex Gaussian random variables with variances $S_X(\omega_m|\theta)$ [36], but since $X(t)$ is real, the sidebands are symmetric with $x_m = x_{-m}^*$. This means that, averaged over x, the photon numbers at opposite sideband frequencies become correlated.

To simplify the analysis, suppose that, for each $m>0$, we sum the pair of measured photon numbers n_m and n_{-m} at opposite sidebands and use a reduced set of measurement record $\{N_m \equiv n_m + n_{-m}; m>0\}$ for estimation. It can be shown that each N_m is also Poissonian conditioned on the mean $2|\alpha|^2|x_m|^2$, but now they remain independent from one another in the set after averaging over $\{x_m; m>0\}$.

With x_m being complex Gaussian and N_m being conditionally Poissonian with mean $2|\alpha|^2|x_m|^2$, it can be shown that the marginal distribution of N_m is a Bose-Einstein distribution [37] with mean number

$$\bar{N}_m = 2|\alpha|^2 S_X(\omega_m|\theta). \tag{3.15}$$

The Fisher information remains analytically tractable and is given by

$$j_{\mu\nu}(P_Y^{(\mathrm{spc})}) = \sum_{m>0}\frac{(\partial_\mu \ln\bar{N}_m)(\partial_\nu\ln\bar{N}_m)}{1+1/\bar{N}_m}. \tag{3.16}$$

If we use the SPLOT assumption to replace $\sum_{m>0}$ with $T\int_0^\infty d\omega/(2\pi)$ [18] and use the symmetry of the integrand to replace $T\int_0^\infty d\omega/(2\pi)$ with $(T/2)\int_{-\infty}^\infty d\omega/(2\pi)$, the Fisher information becomes

$$j_{\mu\nu}\left(P_Y^{(\mathrm{spc})}\right) = T\int_{-\infty}^\infty \frac{d\omega}{2\pi}\frac{(\partial_\mu\ln S_X)(\partial_\nu\ln S_X)}{2+1/(\mathcal{N}S_X)}, \tag{3.17}$$

where $\mathcal{N}$ is the average input photon flux. Since $S_I(\omega) = \mathcal{N}$ for a coherent state, Eq. (3.17) coincides with the quantum bound in Eq. (3.2). This is the second main result of this paper. Comparing Eq. (3.17) with the homodyne limit given by Eq. (3.6), we can expect that spectral photon counting becomes significantly better than homodyne detection when $\mathcal{N}S_X$ is small.

C. Ornstein-Uhlenbeck spectrum analysis

For a more specific example, consider the experiments in Refs. [33, 34], which can be modeled as the continuous-optical-phase-modulation problem depicted in Fig. 1(d), with adaptive homodyne detection depicted in Fig. 2(a) and $X(t)$ given by an Ornstein-Uhlenbeck process. The PSD of $X(t)$ is

$$S_X(\omega|\theta) = \frac{2\theta_1\theta_2}{\omega^2+\theta_2^2}, \tag{3.18}$$

where $\theta_1 = \mathbb{E}_{X|\theta}[X^2(t)]$ is the area under S_X and θ_2 is the bandwidth. The experimental S_I can be assumed to be constant for all frequencies of interest, and the quantum limit given by Eq. (3.2) on the estimation of θ_1 and θ_2 can be computed analytically:

$$\begin{aligned}\tilde{\mathcal{J}}_{11} &= \frac{\theta_2 T}{8\theta_1^2}\frac{C}{\sqrt{1+C/2}},\\ \tilde{\mathcal{J}}_{22} &= \frac{2T}{\theta_2}\frac{1+C/4}{C}\left(\frac{1+C/4}{\sqrt{1+C/2}}-1\right),\\ \tilde{\mathcal{J}}_{12} = \tilde{\mathcal{J}}_{21} &= \frac{T}{2\theta_1}\left(\frac{1+C/4}{\sqrt{1+C/2}}-1\right),\end{aligned} \tag{3.19}$$

where

$$C \equiv \frac{8\theta_1 S_I}{\theta_2} = 4 S_I S_X(0|\theta) \tag{3.20}$$

is an SNR quantity. For comparison, the homodyne limit given by Eq. (3.6) is

$$\begin{aligned}\tilde{j}_{11} &= \frac{\theta_2 T}{8\theta_1^2}\frac{C^2}{(1+C)^{3/2}},\\ \tilde{j}_{22} &= \frac{2T}{\theta_2}\frac{1}{C}\left[\frac{(1+C/2)(1+5C/4+C^2/8)}{(1+C)^{3/2}}\right.\\ &\quad\left.-\left(1+\frac{C}{4}\right)\right],\\ \tilde{j}_{12} = \tilde{j}_{21} &= \frac{T}{2\theta_1}\left[\frac{1+3C/2+C^2/4}{(1+C)^{3/2}}-1\right].\end{aligned} \tag{3.21}$$

For homodyne detection, C is an upper limit on the ratio between the peak of S_X and the homodyne noise floor S_η in the frequency domain.

Figure 3 plots the quantum ($\tilde{\mathcal{J}}^{-1}$) and homodyne ($\tilde{j}^{-1}$) bounds on the estimation errors Σ_{11} and Σ_{22} versus C. Both plots show similar behaviors, and the $C \gg 1$ and $C \ll 1$ limits are of special interest. In the high-SNR regime ($C \gg 1$), both $\tilde{\mathcal{J}}^{-1}$ and $\tilde{j}^{-1}$ approach a C-independent limit:

$$\lim_{C\to\infty}\tilde{\mathcal{J}}^{-1} = \lim_{C\to\infty}\tilde{j}^{-1} = \frac{2}{\theta_2 T}\begin{pmatrix}\theta_1^2 & -\theta_1\theta_2\\ -\theta_1\theta_2 & \theta_2^2\end{pmatrix}, \tag{3.22}$$

and the homodyne performance is near-quantum-optimal. This asymptotic behavior is different from that of the bounds for single-parameter estimation, as both $1/\tilde{\mathcal{J}}_{\mu\mu}$ and $1/\tilde{j}_{\mu\mu}$ scale as $C^{-1/2}$ and decrease indefinitely for increasing C. The matrix bounds thus demonstrate the detrimental effect of having two unknown parameters that act as noise to each other. The C-independent limits also suggest that, once an experiment is in the high-SNR regime, no significant improvement can be made by increasing S_I and reducing the noise floor via photon-flux increase, squeezing, or changing the measurement method.

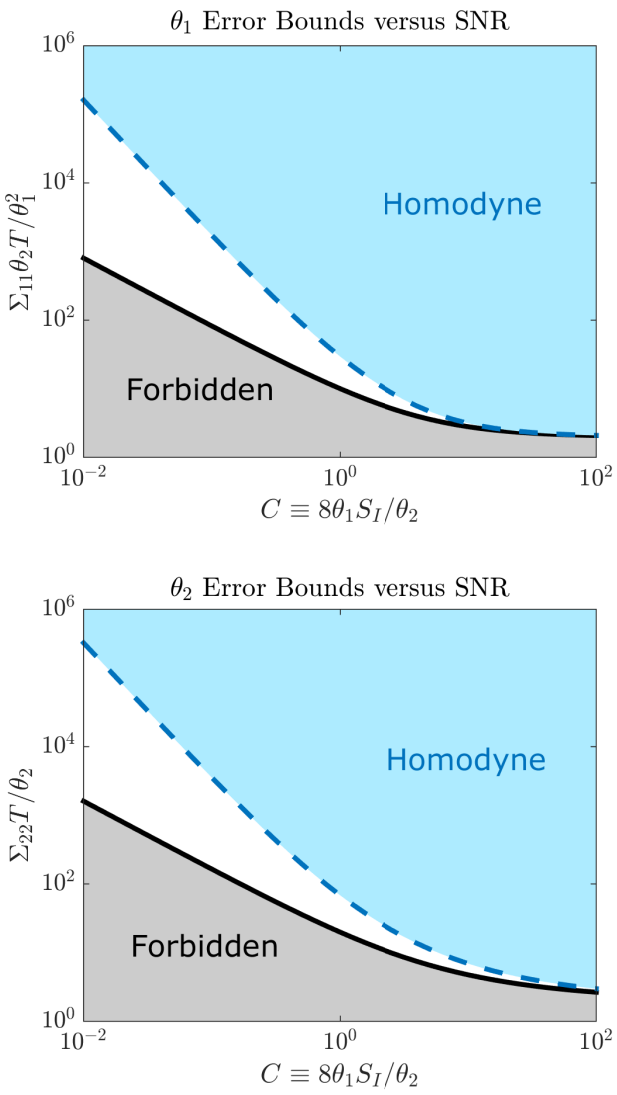

FIG. 3. (Color online). Log-log plots of the quantum limit $\tilde{\mathcal{J}}^{-1}$ (inverse of Eqs. (3.19), black solid line) and homodyne limit $\tilde{j}^{-1}$ (inverse of Eqs. (3.21), blue dashed line) on the mean-square errors versus an SNR quantity $C \equiv 8\theta_1 S_I/\theta_2$. Top plot: limits on Σ_{11} (normalized in a unit of $\theta_1^2/(\theta_2 T)$), bottom plot: limits on Σ_{22} (normalized in a unit of θ_2/T). No measurement can achieve an error below the quantum limit (grey "forbidden" region), while the homodyne performance (blue "homodyne" region) cannot go below the homodyne limit. For $C \gg 1$, the limits approach constants, while for $C \ll 1$ the homodyne limit has a significantly worse error scaling.

In the low-SNR regime ($C \ll 1$), on the other hand, it can be shown that

$$\tilde{\mathcal{J}}^{-1} \approx \frac{8}{\theta_2 T}C^{-1}\begin{pmatrix}\theta_1^2 & 0\\ 0 & 2\theta_2^2\end{pmatrix}, \tag{3.23}$$

$$\tilde{j}^{-1} \approx \frac{16}{\theta_2 T}C^{-2}\begin{pmatrix}\theta_1^2 & \theta_1\theta_2\\ \theta_1\theta_2 & 2\theta_2^2\end{pmatrix}, \tag{3.24}$$

where the homodyne bounds on Σ_{11} and Σ_{22} diverge

from the quantum bounds by a large factor of $2/C \gg 1$. The diverging bounds demonstrate the importance of quantum-optimal measurement in the low-SNR limit: at least for a coherent-state input and weak modulation, the quantum-optimal performance of spectral photon counting can exhibit a superior error scaling and offer significant improvements over homodyne detection.

D. Experimental data analysis

To compare our theory with actual experimental performance, we analyze the data from the experiment reported in Ref. [33], which is in a high-SNR regime ($C \geq 23.5$) and the adaptive homodyne performance is expected to be close to our quantum limit. We focus on the experiment with coherent states and not the one with squeezed states reported in Ref. [34], as Eqs. (3.22) imply that squeezing offers insignificant improvement in this high-SNR regime.

The experiment reported in Ref. [33] used four different mean photon fluxes $\mathcal{N}_1 = 1.315 \times 10^6$ s^{-1}, $\mathcal{N}_2 = 3.616 \times 10^6$ s^{-1}, $\mathcal{N}_3 = 6.327 \times 10^6$ s^{-1}, $\mathcal{N}_4 = 1.418 \times 10^7$ s^{-1}. For each photon flux $\mathcal{N}_k$, M_k traces of $X(t)$ and M_k traces of $Y(t)$ were recorded ($M_1 = 21$, $M_2 = 23$, $M_3 = 24$, $M_4 = 27$). Each trace of $Y(t)$ was obtained using a different feedback gain for the filter in the phase-locked loop, such that the phase locking might not be optimal. The original purpose of varying the feedback gains was to demonstrate the existence of an optimal filter for phase estimation in Ref. [33], but it is also coincidentally appropriate in our present context, as θ_1 and θ_2 are supposed to be unknown here and the optimal filter is not supposed to be known. To make the data analysis tractable, we assume that the phase locking remained tight even if the filter was suboptimal, such that we can still use the linearized model

$$Y(t) = \sin[X(t) - \check{X}(t)] + \eta(t) + \check{X}(t) \approx X(t) + \eta(t), \tag{3.25}$$

where $\check{X}(t)$ is the feedback phase modulation on the local oscillator. Comparisons of the experimental $X(t)$ with $\check{X}(t)$ show that $\mathbb{E}[X(t) - \check{X}(t)]^2 \lesssim 0.3$ and the linearized model is reasonable. Most metrological experiments, such as gravitational-wave detectors, deal with extremely weak phase modulation, so the linearized model is expected to be even more accurate in those cases. Appendix A describes further calibrations to ensure that Eq. (3.25) is accurate.

For any observation time T, the maximum-likelihood estimation can be performed using an expectation-maximization algorithm [36, 42], but our numerical simulations suggest that it is safe here to use a simpler and faster method due to Whittle [43], which exploits the SPLOT assumption to simplify the likelihood function. Consider a real discrete-time series

$$\{Y(t_l); l = 0, 1, \ldots, L-1\}, \quad t_l = l\delta t, \tag{3.26}$$

and zero-mean Gaussian statistics conditioned on θ. Define the discrete Fourier transform as

$$y_m = \frac{\delta t}{\sqrt{T}} \sum_{l=0}^{L-1} Y(t_l) \exp(i\omega_m t_l), \quad \omega_m = \frac{2\pi m}{T}, \tag{3.27}$$

with integer m and $y_m = y^*_{L-m}$. It can be shown that, with the SPLOT assumption, the positive-frequency components $\{y_m; 0 < m < L/2\}$ are independent zero-mean complex Gaussian random variables with variances $S_Y(\omega_m|\theta)$ [36, 43]. This means that the log-likelihood function, up to a θ-independent additive constant $\mathcal{A}$, can be approximated as

$$\ln P_Y \approx \mathcal{A} - \sum_{0<m<L/2} \left[\ln S_Y(\omega_m|\theta) + \frac{|y_m|^2}{S_Y(\omega_m|\theta)} \right]. \tag{3.28}$$

Approximate maximum-likelihood estimation can then be performed by Fourier-transforming the time series into $\{y_m\}$ and finding the parameters that maximize Eq. (3.28). We use Matlab® and its `fft` and `fminunc` functions to implement this procedure on a desktop PC. With $T = 0.01$ s for each $Y(t)$ trace, we expect the SPLOT assumption to be reasonable. We also perform numerical simulations throughout our analysis to ensure that our SPLOT and unbiased-estimator assumptions are valid and our results are expected.

To prevent technical noise and model mismatch at higher frequencies from contaminating our analysis, we consider only the spectral components up to 6×10^5 rad/s $\sim 10\theta_2$, rather than the full measurement bandwidth $\pi/\delta t = \pi \times 10^8$ rad/s. To estimate the true parameters more accurately, we apply the Whittle method to the collective record of all $\sum_k M_k = 95$ experimental $X(t)$ traces, assuming the spectrum given by Eq. (3.18), and obtain $\theta_1 = 0.1323$ and $\theta_2 = 5.909 \times 10^4$ rad/s. We take these to be the true parameters, as the estimates from such a large number of $X(t)$ traces are expected to be much more accurate than those from each $Y(t)$ trace.

We apply the Whittle method to each $Y(t)$ trace and evaluate the estimation errors by comparing the estimates with the true parameters. For each photon flux we assume a noise floor that is estimated from high-frequency data, and then we estimate θ using spectral components of Y up to $\omega = 6 \times 10^5$ rad/s. Let the resulting estimates be

$$\left\{ \check{\theta}^{(m_k)}_{\mu k}; \mu = 1, 2; k = 1, 2, 3, 4; m_k = 1, \ldots, M_k \right\}, \tag{3.29}$$

where μ is the index for the two parameters, k is the index for the photon fluxes, and m_k is the index for the traces, and let the squared distance of each estimate from the true parameter be

$$\varepsilon^{(m_k)}_{\mu k} \equiv \left(\check{\theta}^{(m_k)}_{\mu k} - \theta_\mu \right)^2. \tag{3.30}$$

$\varepsilon_{\mu k}^{(m_k)}$ can be regarded as an outcome for a random variable $\varepsilon_{\mu k}$, so we can use the sample mean

$$\bar{\varepsilon}_{\mu k} \equiv \frac{1}{M_k} \sum_{m_k=1}^{M_k} \varepsilon_{\mu k}^{(m_k)} \tag{3.31}$$

to estimate the expected error

$$\Sigma_{\mu\mu} = \mathbb{E}_Y(\varepsilon_{\mu k}). \tag{3.32}$$

To find the deviation of the sample mean $\bar{\varepsilon}_{\mu k}$ from the expected value, we use an unbiased estimate of the variance of $\varepsilon_{\mu k}$, that is,

$$V_{\mu k} \equiv \frac{1}{M_k - 1} \sum_{m_k=1}^{M_k} \left(\varepsilon_{\mu k}^{(m_k)} - \bar{\varepsilon}_{\mu k}\right)^2, \tag{3.33}$$

and divide it by the number of samples M_k. Our final results

$$\left\{\bar{\varepsilon}_{\mu k} \pm \sqrt{\frac{V_{\mu k}}{M_k}}; \mu = 1, 2; k = 1, 2, 3, 4\right\} \tag{3.34}$$

are plotted in normalized units in Fig. 4, together with the quantum limit given by the inverse of Eqs. (3.19) and the homodyne limit given by the inverse of Eqs. (3.21). The plots demonstrate estimation errors close to both the homodyne limit and the fundamental quantum limit, despite experimental imperfections such as imperfect phase locking.

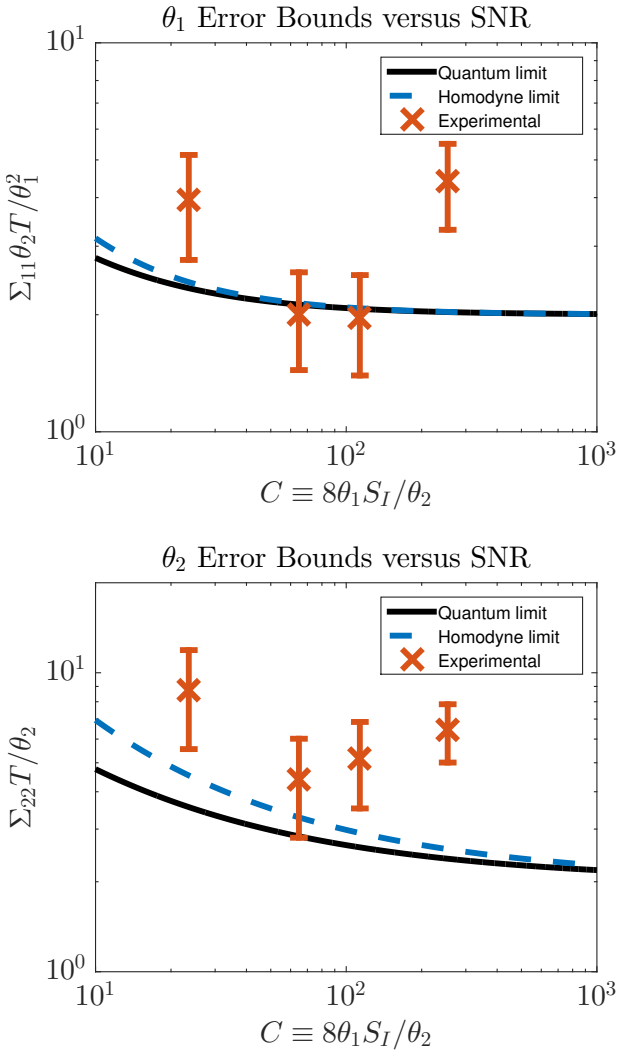

FIG. 4. (Color online). Log-log plots of the quantum limit $\tilde{\mathcal{J}}^{-1}$ (inverse of Eqs. (3.19), black solid line), the homodyne limit $\tilde{j}^{-1}$ (inverse of Eqs. (3.21), blue dash line), and the experimental mean-square estimation errors Σ versus the SNR quantity $C \equiv 8\theta_1 S_I/\theta_2$. Top plot: Experimental $\Sigma_{11} = \{4.0 \pm 1.2, 2.0 \pm 0.6, 2.0 \pm 0.6, 4.4 \pm 1.1\}$ (in a unit of $\theta_1^2/(\theta_2 T)$) versus $C = \{23.5, 64.8, 113, 254\}$, compared with the homodyne limit and the quantum limit. Bottom plot: Experimental $\Sigma_{22} = \{8.7 \pm 3.2, 4.4 \pm 1.6, 5.2 \pm 1.7, 6.4 \pm 1.4\}$ (in a unit of θ_2/T) versus the same C values, compared with the homodyne limit and the quantum limit.

IV. CONCLUSION

We have presented three key results in this paper: a measurement-independent quantum limit to spectrum-parameter estimation, the optimality of spectral photon counting, and an experimental data analysis. The quantum limit applies to a wide range of experiments and is particularly relevant to optomechanics, where the spectrum parameters of a stochastic force are often of interest to gravitational-wave astronomy [3–5, 11]. The proposed spectral photon counting method will be useful whenever the problem can be modeled as weak phase modulation of a coherent state and the SNR is low. Most metrological experiments, including gravitational-wave detectors, involve extremely weak phase modulation and low SNR, so the potential improvement over homodyne or heterodyne detection without the need of squeezed light is an important discovery. Our experimental data analysis further demonstrates the relevance of our theory to current technology and provides a recipe for future spectrum-analysis experiments.

There are many interesting potential extensions of our theory. Although quantum baths can often be modeled classically, a generalization of our formalism to account explicitly for nonclassical baths will make our theory applicable to an even wider range of experiments. A generalization for nonstationary processes and finite observation time will be valuable for the study of unstable systems, which are potentially more sensitive than stable systems [44]. Tighter quantum limits that explicitly account for decoherence may be derived by applying the techniques in Refs. [16, 27, 28]. A Bayesian formulation that removes the unbiased-estimator assumption should be possible [12, 14, 16, 45, 46]. A more detailed study of our theory in the context of optomechanics can serve

as an extension of Refs. [4, 5] and enable a more rigorous analysis of quantum limits to testing wavefunction-collapse models. Application of our theory to spin systems will provide a more rigorous foundation for stochastic magnetometry [29].

The actual performance of spectral photon counting depends on the bandwidth and spectral resolution of the Fourier-transform device, as well as the quantum efficiency and dark counts of the photodetectors in practice. While a more detailed analysis of such practical concerns is needed before one can judge the realistic performance of spectral photon counting with current technology, the large potential improvement in the low-SNR regime indicates the fundamental importance of coherent optical information processing for sensing applications and should motivate further technological advances in coherent quantum optical devices [10, 38, 47–51]. In the high-SNR regime, on the other hand, our theory and experimental data analysis suggest that current technology can already approach the quantum limits with homodyne or even heterodyne detection. In this regime, our quantum limit primarily serves as a no-go theorem, proving that no other measurement can offer significant improvement. The challenge for actual metrological experiments will be to reach the high-SNR regime for weak signals, in which case our theory should serve as a rigorous foundation to guide future experimental designs.

ACKNOWLEDGMENTS

We acknowledge helpful discussions with Ranjith Nair and Xiao-Ming Lu. This work is supported in part by the Singapore National Research Foundation under NRF Grant No. NRF-NRFF2011-07, Singapore Ministry of Education Academic Research Fund Tier 1 Project R-263-000-C06-112, the Australian Research Council, Grant No. CE1101027, PDIS, GIA, APSA commissioned by the MEXT of Japan, ASCR-JSPS and the SCOPE program of the MIC of Japan, CREST of JST.

Appendix A: Experimental data recalibration

In the experiment described in Ref. [33], calibration procedures were used to convert applied and measured voltages to the various physical quantities defined throughout Ref. [33]. In the course of analysing that experimental data for the purposes of the new estimation task described here, we found that the data gives non-negligible bias in the estimation of θ_1. It turns out that the original calibration of experimental data was not accurate enough for the new task of estimating θ_1 (note that θ_2 is robust against this inaccuracy). The systematic calibration error had insignificant effects on the phase estimation task in Ref. [33] – making the estimate slightly worse than it would have been without the bias but generally within the uncertainty of the experiment as reported in Ref. [33]. The bias might have been caused by non-linearity or saturation of electronic circuits during the calibration phase of the experiment or long timescale drift. For the purpose of this new estimation task, we refine the calibration of the data from Ref. [33] so that we can achieve an accurate estimate. To do this in a fair way we use two extra data sets ($k = 5, 6$), which were not shown in Ref. [33] but recorded by the same experimental setup with different experimental parameters. Mean photon fluxes of these data sets are $\mathcal{N}_5 = 6.198\times10^6$ s^{-1} and $\mathcal{N}_6 = 5.986\times10^6$ s^{-1}. Number of traces are $M_5 = 24$ and $M_6 = 24$. Note that we use these "training" data only for the purposes of refining the experimental calibration. We apply the Whittle method to the two extra data sets to obtain the true θ_1 from the collective record of $X(t)$, and a mean value of the estimated θ_1 from the collective record of $Y(t)$ traces using the coarse calibration from Ref. [33]. We determine that a refined calibration factor of 0.8945 is required to cancel the unwanted bias in the estimate of θ_1 for the extra data sets $k = 5, 6$. We then apply the refined calibration factor to $Y(t)$ of the original data sets ($k = 1$ to 4). By this method, we can refine the calibration of the original data presented in Ref. [33] by making use of independent, but contemporaneously recorded data.

[1] Markus Aspelmeyer, Tobias J. Kippenberg, and Florian Marquardt, "Cavity optomechanics," Rev. Mod. Phys. **86**, 1391–1452 (2014).
[2] Vladimir B. Braginsky and Farid Ya. Khalili, *Quantum Measurement* (Cambridge University Press, Cambridge, 1992).
[3] The LIGO Scientific Collaboration & The Virgo Collaboration, "An upper limit on the stochastic gravitational-wave background of cosmological origin," Nature **460**, 990–994 (2009).
[4] Stefan Nimmrichter, Klaus Hornberger, and Klemens Hammerer, "Optomechanical sensing of spontaneous wave-function collapse," Phys. Rev. Lett. **113**, 020405 (2014).
[5] Lajos Diósi, "Testing spontaneous wave-function collapse models on classical mechanical oscillators," Phys. Rev. Lett. **114**, 050403 (2015).

[6] Thomas M. Stace, "Quantum limits of thermometry," Phys. Rev. A **82**, 011611 (2010).

[7] Ugo Marzolino and Daniel Braun, "Precision measurements of temperature and chemical potential of quantum gases," Phys. Rev. A **88**, 063609 (2013).

[8] M. Jarzyna and M. Zwierz, "On quantum interferometric measurements of temperature," ArXiv e-prints (2014), arXiv:1412.5609 [quant-ph].

[9] Luis A. Correa, Mohammad Mehboudi, Gerardo Adesso, and Anna Sanpera, "Individual quantum probes for optimal thermometry," Phys. Rev. Lett. **114**, 220405 (2015).

[10] Ranjith Nair and Mankei Tsang, "Quantum optimality of photon counting for temperature measurement of thermal astronomical sources," The Astrophysical Journal **808**, 125 (2015).

[11] B. P. Abbott *et al.* (LIGO Scientific Collaboration and Virgo Collaboration), "Observation of gravitational waves from a binary black hole merger," Phys. Rev. Lett. **116**, 061102 (2016).

[12] Harry L. Van Trees, *Detection, Estimation, and Modulation Theory, Part I.* (John Wiley & Sons, New York, 2001).

[13] Michael A. Nielsen and Isaac L. Chuang, *Quantum Computation and Quantum Information* (Cambridge University Press, Cambridge, 2011).

[14] Mankei Tsang, Howard M. Wiseman, and Carlton M. Caves, "Fundamental quantum limit to waveform estimation," Phys. Rev. Lett. **106**, 090401 (2011).

[15] Mankei Tsang and Ranjith Nair, "Fundamental quantum limits to waveform detection," Phys. Rev. A **86**, 042115 (2012).

[16] Mankei Tsang, "Quantum metrology with open dynamical systems," New Journal of Physics **15**, 073005 (2013).

[17] Christopher E. Granade, Christopher Ferrie, Nathan Wiebe, and D. G. Cory, "Robust online Hamiltonian learning," New Journal of Physics **14**, 103013 (2012).

[18] Carl W. Helstrom, *Quantum Detection and Estimation Theory* (Academic Press, New York, 1976).

[19] Alexander S. Holevo, *Probabilistic and Statistical Aspects of Quantum Theory* (Edizioni della Normale, Pisa, Italy, 2011).

[20] M. Hayashi, *Quantum Information* (Springer, Berlin, 2006).

[21] Matteo Brunelli, Stefano Olivares, and Matteo G. A. Paris, "Qubit thermometry for micromechanical resonators," Phys. Rev. A **84**, 032105 (2011).

[22] Claudia Benedetti, Fabrizio Buscemi, Paolo Bordone, and Matteo G. A. Paris, "Quantum probes for the spectral properties of a classical environment," Phys. Rev. A **89**, 032114 (2014).

[23] Søren Gammelmark and Klaus Mølmer, "Fisher information and the quantum cramér-rao sensitivity limit of continuous measurements," Phys. Rev. Lett. **112**, 170401 (2014).

[24] S. Alipour and A. T. Rezakhani, "Extended convexity of quantum fisher information in quantum metrology," Phys. Rev. A **91**, 042104 (2015).

[25] O. E. Barndorff-Nielsen and R. D. Gill, "Fisher information in quantum statistics," Journal of Physics A: Mathematical and General **33**, 4481 (2000).

[26] Thomas Kailath, "The divergence and Bhattacharyya distance measures in signal selection," IEEE Transactions on Communication Technology **15**, 52–60 (1967).

[27] R. Demkowicz-Dobrzański, J. Kołodyński, and M. Guţă, "The elusive Heisenberg limit in quantum-enhanced metrology," Nature Communications **3**, 1063 (2012).

[28] B. M. Escher, R. L. de Matos Filho, and L. Davidovich, "General framework for estimating the ultimate precision limit in noisy quantum-enhanced metrology," Nature Physics **7**, 406–411 (2011).

[29] L. T. Hall, J. H. Cole, C. D. Hill, and L. C. L. Hollenberg, "Sensing of fluctuating nanoscale magnetic fields using nitrogen-vacancy centers in diamond," Phys. Rev. Lett. **103**, 220802 (2009).

[30] A. De Pasquale, D. Rossini, P. Facchi, and V. Giovannetti, "Quantum parameter estimation affected by unitary disturbance," Phys. Rev. A **88**, 052117 (2013).

[31] Harry L. Van Trees, *Detection, Estimation, and Modulation Theory, Part III: Radar-Sonar Signal Processing and Gaussian Signals in Noise* (John Wiley & Sons, New York, 2001).

[32] Howard M. Wiseman and Gerard J. Milburn, *Quantum Measurement and Control* (Cambridge University Press, Cambridge, 2010).

[33] T. A. Wheatley, D. W. Berry, H. Yonezawa, D. Nakane, H. Arao, D. T. Pope, T. C. Ralph, H. M. Wiseman, A. Furusawa, and E. H. Huntington, "Adaptive optical phase estimation using time-symmetric quantum smoothing," Phys. Rev. Lett. **104**, 093601 (2010).

[34] Hidehiro Yonezawa, Daisuke Nakane, Trevor A. Wheatley, Kohjiro Iwasawa, Shuntaro Takeda, Hajime Arao, Kentaro Ohki, Koji Tsumura, Dominic W. Berry, Timothy C. Ralph, Howard M. Wiseman, Elanor H. Huntington, and Akira Furusawa, "Quantum-enhanced optical-phase tracking," Science **337**, 1514–1517 (2012).

[35] Kohjiro Iwasawa, Kenzo Makino, Hidehiro Yonezawa, Mankei Tsang, Aleksandar Davidovic, Elanor Huntington, and Akira Furusawa, "Quantum-limited mirror-motion estimation," Phys. Rev. Lett. **111**, 163602 (2013).

[36] Robert H. Shumway and David S. Stoffer, *Time Series Analysis and Its Applications* (Springer, New York, 2006).

[37] Daniel F. Walls and Gerard J. Milburn, *Quantum Optics* (Springer-Verlag, Berlin, 2008).

[38] Mankei Tsang, "Quantum nonlocality in weak-thermal-light interferometry," Phys. Rev. Lett. **107**, 270402 (2011).

[39] Jeffrey H. Shapiro, "Quantum measurement eigenkets for continuous-time direct detection," Quantum and Semiclassical Optics: Journal of the European Optical Society Part B **10**, 567 (1998).

[40] David J. Brady, *Optical Imaging and Spectroscopy* (Wiley, Hoboken, 2009).

[41] S. T. Chu, B. E. Little, W. Pan, T. Kaneko, S. Sato, and Y. Kokubun, "An eight-channel add-drop filter using vertically coupled microring resonators over a cross grid," IEEE Photonics Technology Letters **11**, 691–693 (1999).

[42] Shan Zheng Ang, Glen I. Harris, Warwick P. Bowen, and Mankei Tsang, "Optomechanical parameter estimation," New Journal of Physics **15**, 103028 (2013).

[43] P. Whittle, "The analysis of multiple stationary time series," Journal of the Royal Statistical Society. Series B (Methodological) **15**, pp. 125–139 (1953).

[44] Mankei Tsang, "Quantum transition-edge detectors," Phys. Rev. A **88**, 021801(R) (2013).

[45] Mankei Tsang, "Ziv-Zakai error bounds for quantum parameter estimation," Phys. Rev. Lett. **108**, 230401

(2012).

[46] Dominic W. Berry, Mankei Tsang, Michael J. W. Hall, and Howard M. Wiseman, "Quantum Bell-Ziv-Zakai Bounds and Heisenberg Limits for Waveform Estimation," Phys. Rev. X **5**, 031018 (2015).

[47] Jacques Carolan, Christopher Harrold, Chris Sparrow, Enrique Martín-López, Nicholas J. Russell, Joshua W. Silverstone, Peter J. Shadbolt, Nobuyuki Matsuda, Manabu Oguma, Mikitaka Itoh, Graham D. Marshall, Mark G. Thompson, Jonathan C. F. Matthews, Toshikazu Hashimoto, Jeremy L. O'Brien, and Anthony Laing, "Universal linear optics," Science **349**, 711–716 (2015).

[48] Daniel Gottesman, Thomas Jennewein, and Sarah Croke, "Longer-baseline telescopes using quantum repeaters," Phys. Rev. Lett. **109**, 070503 (2012).

[49] Mankei Tsang, Ranjith Nair, and Xiao-Ming Lu, "Quantum theory of superresolution for two incoherent optical point sources," ArXiv e-prints (2015), arXiv:1511.00552 [quant-ph].

[50] Ranjith Nair and Mankei Tsang, "Interferometric superlocalization of two incoherent optical point sources," Opt. Express **24**, 3684–3701 (2016).

[51] Mankei Tsang, Ranjith Nair, and Xiao-Ming Lu, "Semiclassical Theory of Superresolution for Two Incoherent Optical Point Sources," ArXiv e-prints (2016), arXiv:1602.04655 [quant-ph].